Article

The Interplay between Experimental Data and Uncertainty Analysis in Quantifying CO_2 Trapping during Geological Carbon Storage

Marcos Vitor Barbosa Machado [1,*], Mojdeh Delshad [2] and Kamy Sepehrnoori [2]

[1] PETROBRAS, Rio de Janeiro, RJ 20231-030, Brazil

[2] Hildebrand Department of Petroleum and Geosystems Engineering, The University of Texas at Austin, Austin, TX 78712, USA; delshad@mail.utexas.edu (M.D.); kamys@mail.utexas.edu (K.S.)

* Corresponding author. E-mail: marcosbarbosa@petrobras.com.br (M.V.B.M.)

ABSTRACT: Numerical simulation is a widely used tool for studying CO_2 storage in porous media. It enables the representation of trapping mechanisms and CO_2 retention capacity. The complexity of the involved physicochemical phenomena necessitates multiphase flow, accurate fluid and rock property representation, and their interactions. These include CO_2 solubility, diffusion, relative permeabilities, capillary pressure hysteresis, and mineralization, all crucial in CO_2 trapping during carbon storage simulations. Experimental data is essential to ensure accurate quantification. However, due to the extensive data required, modeling under uncertainty is often needed to assess parameter impacts on CO_2 trapping and its interaction with geological properties like porosity and permeability. This work proposes a framework combining laboratory data and stochastic parameter distribution to map uncertainty in CO_2 retention over time. Published data representing solubility, residual trapping, and mineral trapping are used to calibrate prediction models. Geological property variations, like porosity and permeability, are coupled to quantify uncertainty. Results from a saline sandstone aquifer model demonstrate significant variation in CO_2 trapping, ranging from 17% (P10 estimate) to 56% (P90), emphasizing the importance of considering uncertainty in CO_2 storage projects. Quadratic response surfaces and Monte Carlo simulations accurately capture this uncertainty, resulting in calibrated models with an R-squared coefficient above 80%. In summary, this work provides a practical and comprehensive framework for studying CO_2 retention in porous media, addressing uncertainty through stochastic parameter distributions, and highlighting its importance in CO_2 storage projects.

Keywords: CO_2 trapping mechanisms; CCS; Uncertainty analysis; Proxy models; Saline aquifer

1. Introduction

Scenarios considered by international entities such as the International Agency (IEA) point out the complexity of the actions needed to achieve the goals established for reducing emissions of Greenhouse Gases, in the coming decades, simultaneously with the desired transformation in energy generation sources. The report "World Energy Outlook 2022" [1] emphasizes that multiple technologies and energy sources will play an essential role in providing energy resources for the planet in a more sustainable scenario. Among the various options for reducing CO_2 emissions, Carbon Capture and Storage (CCS) presents itself as a technology with significant potential to reduce CO_2 emissions in a probable scenario of continued use of fossil fuels in the coming decades.

A CCS project involves CO_2 capture from high-emission industries and injecting it into geological formations such as saline aquifers and depleted hydrocarbon reservoirs. One of the most critical barriers to long-term and large-volume CO_2 storage in geological formations is the proof of safe and reliable storage. For that, CO_2 can take advantage of different trapping mechanisms in porous media [2–6]; for example, free CO_2 migration is controlled by the structural and stratigraphic trapping exerted by the caprock during the short-term encompassing the injection time, known as a primary mechanism [7]. Part of that mobile CO_2 will be dissolved in the water (solubility trapping) as time passes. This CO_2 solubility trapping is more pronounced in low-salinity brine, high-pressure, and low-temperature conditions [8,9]. The rising plume changes CO_2 saturation leading to an increase in capillary trapped volume due to hysteresis in relative permeability and capillarity [10]. Some CO_2 can be trapped as minerals because of brine pH reduction by CO_2 injection

of the brine and the mineralogy of the rock [11], on a timescale of more than 100,000 years [5]. Therefore, those additional mechanisms increase storage security when the buoyant CO_2 is immobile in the pore space or no longer exists as a free phase (generally, as super-critical CO_2).

Modeling CO_2 retention in porous media depends on the reservoir rock properties, such as porosity and permeability, as well as intrinsic parameters related to each trapping mechanism. These parameters can be measured in lab experiments using reservoir cores and reservoir brine samples. This data helps reduce the uncertainty in the amount of CO_2 that will be trapped in a CCS project. However, it is important to note that a complete and single suite of lab data is not always available, or it may not fully capture the system's heterogeneity, resulting in inherent modeling uncertainty [12]. Therefore, evaluating storage uncertainty involves assessing associated risks by considering modeling parameter uncertainties and system variability, enabling better understanding and management of CO_2 storage risks.

To address the evaluation of uncertainties in the context of CCS, various authors have focused on assessing uncertainties related to geological property distributions [13,14], such as porosity and permeability. Some studies have gone further by incorporating intrinsic parameters of CO_2 trapping in their evaluations [15–18]. For instance, Jammoul et al. [17] conducted a history-matching study to reproduce experimental data while considering uncertainties. Similarly, Likanapaisal et al. [18] investigated the influence of rock and fluid properties, as well as grid size, on the shape of the CO_2 plume. In their work, they specifically examined uncertainties related to the geometry of the CO_2 plume, simplifying the modeling of trapping mechanisms by adopting a black-oil model.

In this study, a framework for uncertainty analysis in CO_2 retention in porous media is proposed. It integrates petrophysical properties and comprehensive trapping modeling, utilizing data collected from published laboratory studies. By doing so, it is possible to accurately quantify both trapped and free CO_2 volumes, enabling a thorough analysis at a field scale with simulations spanning hundreds of years (long-term assessment). This is in contrast to previous studies [17], which focused on short-term redistribution over a few days in a smaller-scale lab model.

Our study also emphasizes the importance of conducting risk assessments in geological carbon storage projects. It takes a comprehensive approach to characterize CO_2 trapping mechanisms, including solubility, residual, and mineral trapping. This is achieved by leveraging lab data to establish distributions and relationships between parameters and geological properties. This unique approach sets our study apart from other studies conducted by different authors [15,16].

2. Modeling Trapping Mechanisms and Their Intrinsic Uncertainties

2.1. Solubility Trapping

The solubility of CO_2 in brine is Influenced by pressure, temperature, and salinity [8]. Several models have been developed to describe this relationship, such as those based on the Peng-Robinson Equation-of-state (EoS) and Henry's law, as seen in [19] and [20]. Other models, like the one proposed by Duan and Sun [9], consider the EoS and the chemical potential of CO_2 in both the liquid and vapor phases.

This study will use the Li and Nghiem model [19], which is available in the CMG-GEM compositional simulator [21]. This model has been calibrated using published experimental data and it calculates Henry's constant based on Equation (1), which takes into account pressure and temperature. Additionally, the impact of salt on gas solubility in the aqueous phase is accounted for by the salting-out coefficient [22].

$$\ln(H_i) = \ln(H_i^*) + \frac{\overline{v}_l}{RT}(p - p^*) \tag{1}$$

where
H_i: Henry's constant at current pressure (p) and temperature (T);
H_i^*: Henry's constant at reference pressure (p^*) and temperature (T);
$\overline{v}_l$: partial molar volume at infinite dilution;
R: universal gas constant;
i: species dissolved in water (CO_2 in this work).

The parameters H_i^* and $\overline{v}_l$ can be adjusted to better fit the experimental solubility data and address any discrepancies in the model predictions. In this study, two levels of solubility were considered: 58,000 ppm at 50 °C [23] and 232,000 ppm at 80 °C [9]. As shown in Figure 1, the default values of H_i^* and $\overline{v}_l$ in Li and Nghiem model provide good agreement with the experimental results for the lower salinity case of 58,000 ppm. However, Figure 2 indicates that a tuning step is necessary to calibrate this model with the laboratory data when the brine salinity is higher than 230,000 ppm.

Table 1 provides a summary of the changes in the regression parameters for each salinity case. These variations will be employed to quantify and prioritize the impact of the uncertainty in this parameter on the estimation of trapped CO_2. This is particularly significant in the absence of laboratory data to use for solubility calculations.

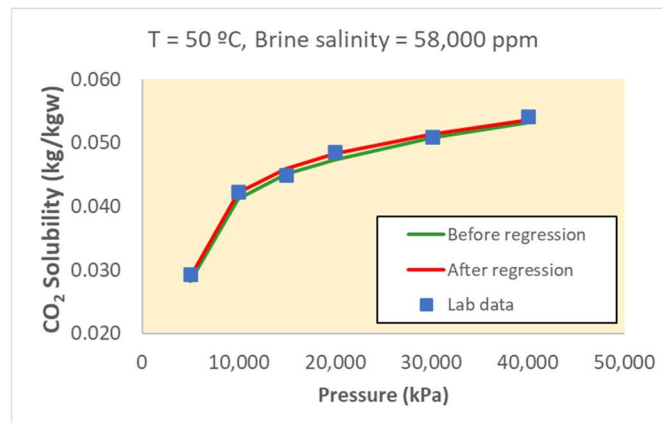The synthetic water compositions are represented in Table 2.

Figure 1. CO_2 solubility in brine with 58,000 ppm at 50 °C (in blue dots [23]) and prediction with Li and Nghiem model with default parameters (green curve) and after regression (red curve).

Figure 2. CO_2 solubility in brine with 230,000 ppm at 80 °C (in blue dots [9]) and prediction with Li and Nghiem model with default parameters (green curve) and after regression (red curve).
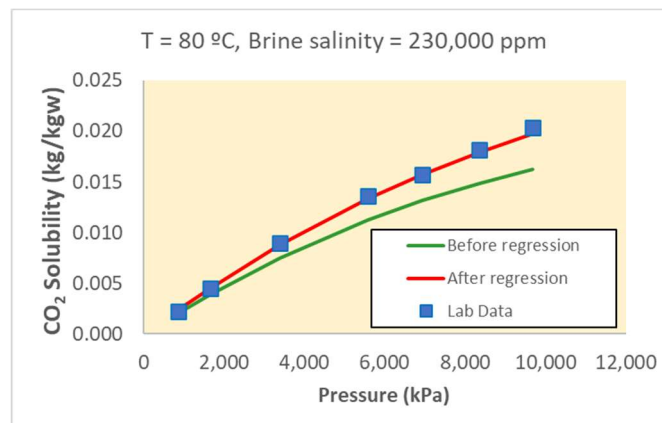
Table 1. Solubility parameter changes for each salinity case.

Cases	Before Regression	After Regression
58,000 ppm at 50 °C	$H_i^* = 3.69 \times 10^5$ at 10 MPa $\bar{v}_l = 3.5 \times 10^{-2}$ L/mol	$H_i^* = 2.91 \times 10^5$ at 10 MPa $\bar{v}_l = 3.665 \times 10^{-2}$ L/mol
230,000 ppm at 80 °C	$H_i^* = 1.02 \times 10^6$ at 8 MPa $\bar{v}_l = 3.5 \times 10^{-2}$ L/mol	$H_i^* = 3.81 \times 10^5$ at 8 MPa $\bar{v}_l = 2.0 \times 10^{-2}$ L/mol

Table 2. Ionic composition of formation brines.

Ions	Concentration (mol/kgw)	
	58,000 ppm case	**230,000 ppm case**
H^+	1.95618×10^{-6}	1.95618×10^{-6}
Ca^{2+}	0.30308	0.30308
Mg^{2+}	0.04185	0.04185
Na^+	0.3234	1.8124
Cl^-	0.551	2.78964
HCO_3^-	0.007482	0.007482

In relation to solubility trapping, the dissolution of CO_2 into brine can be accelerated by molecular diffusion through natural convection, as observed in the study by Rezk et al. [24]. This phenomenon significantly increases the overall storage rate in the aquifer, as fresh brine is brought to the top by convection currents. To assess the importance of molecular diffusion on storage results, a uniformly distributed effective diffusion coefficient of supercritical CO_2 in water ranging from 3.5×10^{-5} to 4.0×10^{-5} cm²/s, based on the work of Ahmadi et al. [25], is used. This distribution

encompasses the uncertainty arising from the dependence of the diffusion coefficient on temperature, pressure, and CO_2 phase alteration (from gas to supercritical phase). However, it should be noted that it does not account for the potential variation of diffusion coefficient with brine salinity [26]. This is primarily due to the challenge of obtaining a comprehensive laboratory dataset that considers all these parameters.

2.2. Residual Trapping

The residual trapping of CO_2 resulting from relative permeability - capillary pressure - saturation hysteresis, was modeled using the two-phase Carlson's model [27] with the maximum trapped gas (S_{gt}) converted to the Land's constant (C) [28] in the two-phase Carlson's model [27], as recommended by Jarrell et al. [29], according to Equation (2):

$$S_{gt} = \frac{S_{g\,max}}{1 + CS_{g\,max}} \tag{2}$$

where $S_{g\,max}$ is the maximum gas saturation.

To capture the variability of S_{gt} in sandstone, Burnside and Naylor [10] gathered data from over 30 published CO_2-brine coreflood experiments. Using the published data, a distribution of S_{gt} (as depicted in Figure 3) is established and employed to assess its impact on the amount of residual CO_2 trapped.

The study by Burnside and Naylor [10] also presents a relationship between the endpoint relative permeability of CO_2 (Max CO_2 k_r) and rock (absolute) permeability as shown in Figure 4. To account for the variability in rock permeability within geological uncertainties, the Max CO_2 k_r will be updated according to the permeability assigned to each gridblock. This ensures that the relative permeability curves can be adjusted accordingly for each gridblock in the uncertain geological scenarios considered in the study.

The residual water saturation (S_{wr}) is a critical parameter for determining the drainage relative permeability curves (k_r) in two-phase CO_2 and brine flow. Burnside and Naylor [10] measured a wide range of values for S_{wr}. A continuous uniform distribution ranging from 0.15 to 0.5 was assumed for the subsequent steps in this study. Additionally, the hysteresis model proposed by Carlson [27] was considered in this study to generate the imbibition k_r - P_c - S_w curves.

In order to ensure consistency between the CO_2-brine capillary pressure curves (P_c), k_r, and the assigned S_{gt}, a script was developed. This script builds the P_c curves based on the power-law equation proposed by Brooks and Corey [30]. Equations 3 and 4 were used for the drainage and imbibition cycles, respectively. For the imbibition curve, the equation was adapted to respect the S_{gt} value as an endpoint k_r (Figure 5). This adaptation ensures that the P_c curves are consistent with the S_{gt} value.

$$P_{c,d} = \left(Max\ P_c\ - P_c^{S_{g\,crit}} \right) \left(\frac{1 - S_{g\,crit} - S_w}{1 - S_{g\,crit} - S_{wr}} \right)^{exp,d} + Min\ P_{c,d} \tag{3}$$

$$P_{c,i} = \left(Max\ P_c\ \right) \left(\frac{1 - S_{gt} - S_w}{1 - S_{gt} - S_{wr}} \right)^{exp,i} \tag{4}$$

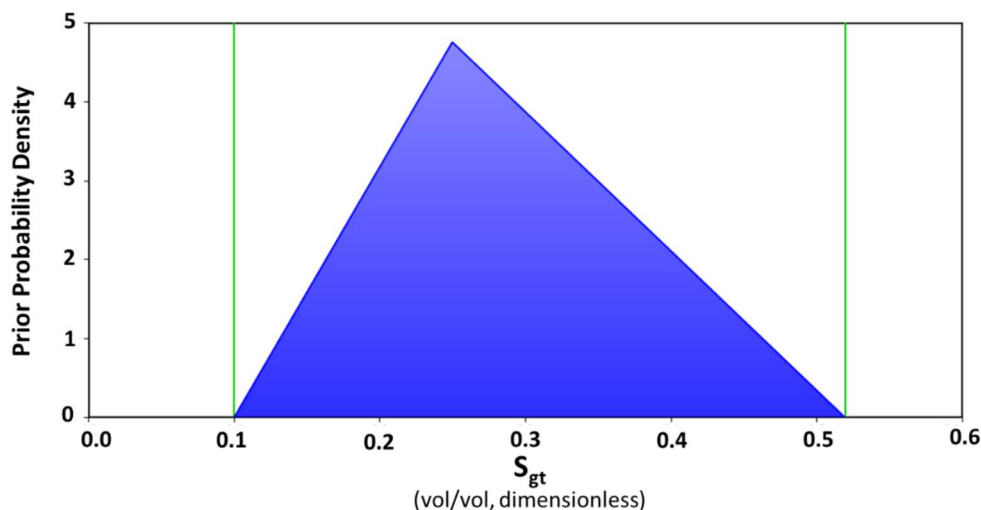where $S_{g\,crit}$ is the critical gas saturation.

Figure 3. Prior S_{gt} distribution built with data collected by Burnside and Naylor [10]. The vertical green lines in the graph indicate the range of variation for S_{gt}.
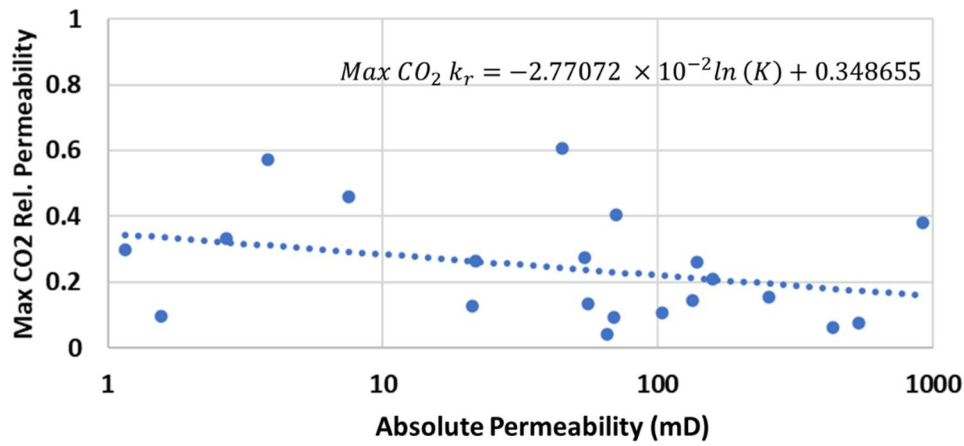
$$Max\ CO_2\ k_r = -2.77072 \times 10^{-2} ln\ (K) + 0.348655$$

Figure 4. Relationship between CO_2 k_r endpoint and the rock permeability based on the data collected by [10].
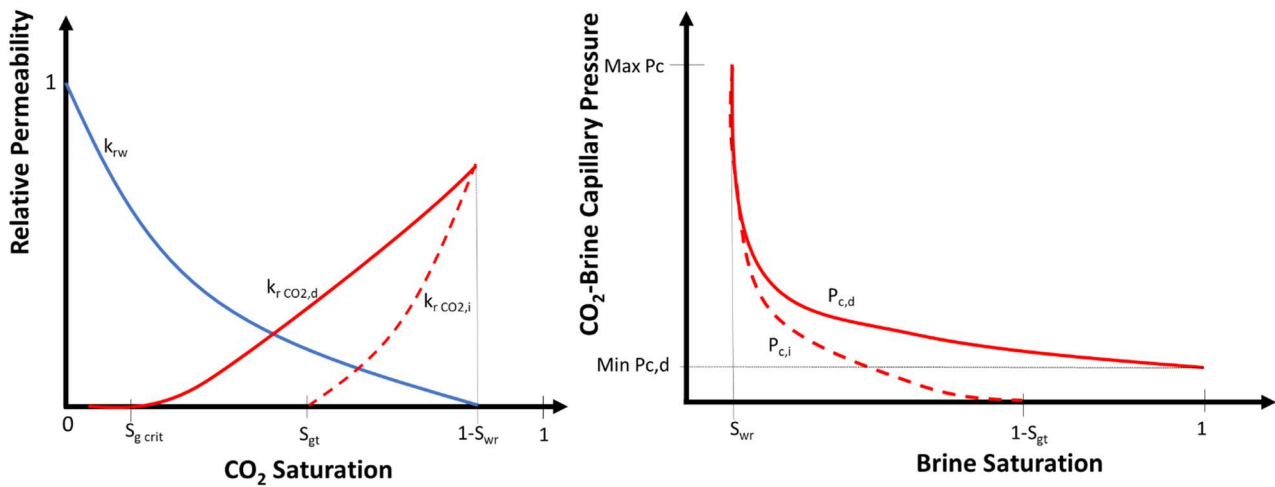

Figure 5. Schematic of CO_2 and brine Relative Permeability ($k_{r\ CO_2}$ and k_{rw}) and Capillary Pressure (P_c) curves for drainage (subscript *d*) and imbibition (subscript *i*) processes.

In the course of numerical simulations, the P_c curves are calculated using J-functions [31]. These curves are then denormalized according to the rock permeability and porosity from the respective uncertain geological scenario. The resulting drainage k_r and drainage/imbibition P_c curves are shown in Figure 6.
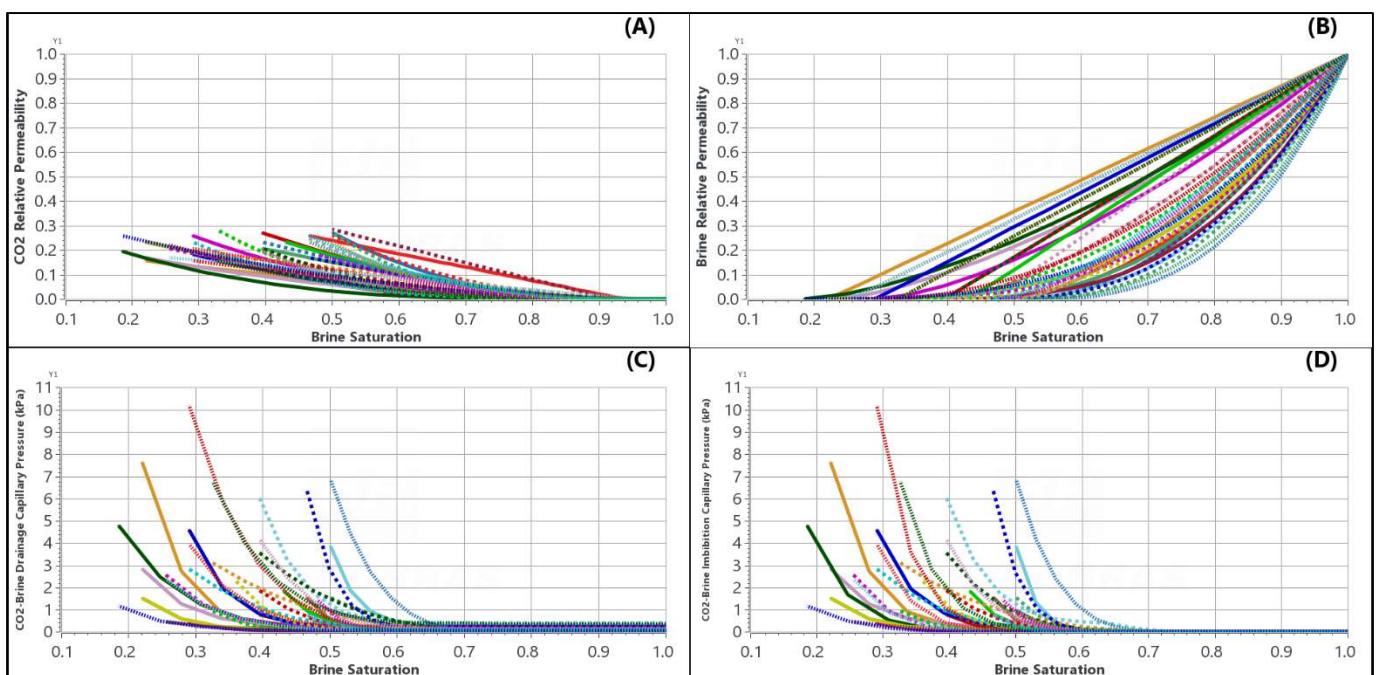

Figure 6. Drainage relative permeability curves for CO_2 (**A**) and brine (**B**) and drainage (**C**) and imbibition (**D**) capillary pressure curves, in kPa, for CO_2 and brine.

The curves in Figure 6 take into account the assumed distribution for S_{gt} (as depicted in Figure 3), the dependency of endpoint CO_2 k_r on rock permeability (as illustrated in Figure 4), and the P_c derived from the J-function considering various permeability and porosity values. Ranges of exponents were assigned based on laboratory data for the generation of relative permeability [32] and capillary pressure [33,34] curves. The table summarizing these ranges will be presented in the next section (Table 5), and the resulting curves will be used in the uncertainty analysis step of the study.

In the current geo-model under investigation, the dry-out effect resulting from water vaporization, particularly around the well, has not been taken into consideration. However, the impact of this dry-out effect on injectivity has been studied by Machado et al. [35]. To model the dry-out effect, it is necessary to extrapolate the P_c curves to lower water saturation values ($<S_{wr}$). Melrose [36] suggested a linear trend of P_c with the $\ln(S_w)$ when water is the wetting phase. This trend can guide the extrapolation process.

2.2. Mineral Trapping

In this case, calcite cementation within the sandstone pores is assumed to be 1.1% [37]. The calcite reaction with CO_2 can result in its dissolution and/or further precipitation. This process is governed by reactions occurring at the mineral/brine interface as follows:

- The acidic reactions leading to bicarbonate and carbonate ions are controlled by kinetic parameters obtained from the PHREEQC database [38,39]:

$$OH^- + H^+ = H_2O \tag{5}$$

$$CO_2 + H_2O = H^+ + HCO_3^- \tag{6}$$

$$CO_3^{2-} + H^+ = HCO_3^- \tag{7}$$

- Reactions with primary minerals, using the Transition-State-Theory (TST)-derived rate laws [40]:

$$Calcite\ [CaCO_3] + H^+ = Ca^{2+} + HCO_3^- \tag{8}$$

Considering the findings of Machado et al. [35,41], it has been determined that only the reaction involving calcite will be included in the model. This decision is based on the fact that the other low-reactivity primary minerals, namely Quartz, K-feldspar, and Plagioclase, do not exhibit significant changes within the evaluated timeframe. The calcite reaction is regulated by four parameters, with three of them having similar values based on data obtained from open databases (PHREEQC: [38,39]; MINTEQ: [42]; WOLERY: [43]). However, the reactive surface area (A) changed considerably in value among different authors due to its dependence on the grain size diameter of the reactive minerals in the rock [44,45], especially in a clastic rock, such as sandstone, where the reactive surface area of an individual mineral grain is dependent on its grain size.

- K_{eq} is the chemical equilibrium constant for the calcite reaction;
- A is the reactive surface area for calcite;
- k_{25} is the rate constant of the calcite reaction at 25 °C (reference);
- E_a is the activation energy.

Table 3 presents a summary of kinetic values obtained from the literature survey that are used in the uncertainty evaluation.

After presenting the trapping modeling, it is worth stating the main assumptions in this paper.

- No geomechanical modeling;
- Pure CO_2 stream is injected, e.g., without impurities and free water content;
- No dry-out effect modeling due to water vaporization with CO_2 injection;
- No rock wettability changes;
- No dependence of the diffusion on brine salinity;
- Simplified geochemical modeling, only considering the calcite dissolution reaction;
- The focus on the technical subsurface phenomena related to CO_2 retention in porous media. It does not include the assessment of risks and uncertainties associated with surface processes [46], process efficiency [47,48], or economic aspects [49].

Table 3. Kinetic parameters of TST model for calcite reaction.

Parameter	Value/Range	Source
$\log_{10}(K_{eq})$	−8.66	PHREEQC database [38,39]
A	83.8 to 23,000 m^2/m^3	[44]
$\log_{10}(k_{25})$	−8.48 mol/m^2s	PHREEQC database [38,39]
E_a	14,400 J/mol	PHREEQC database [38,39]

3. Uncertain Geological Scenarios and Results

The final evaluation of the CO_2 storage potential in the sandstone aquifer was performed using a model based on actual seismic and well data from three wells in the Campos Basin, located in the state of Rio de Janeiro, Brazil. The aquifer covers both onshore and offshore areas. The sand grains in the aquifer are primarily composed of quartz and feldspars, with a notable presence of granitic lithoclasts, which are mechanically formed and deposited fragments of rock derived from older rocks. The average porosity of the sandstone is approximately 20%, and it is primarily generated through secondary processes such as matrix contraction, grain dissolution, or grain fracturing. The average permeability of the aquifer is around 2 Darcy.

To evaluate the CO_2 storage potential, 75 different petrophysical properties (some examples are given in Figure 7) are considered. Different realizations of permeability and porosity are generated to capture the variability and uncertainty in these properties (Personal communication with PETROBRAS, 2023) and final CO_2 retention.

These simulations provide insights into the potential capacity and effectiveness of CO_2 storage in the sandstone aquifer, considering the range of geological and trapping properties observed in the region. This information is crucial for assessing the feasibility and long-term stability of CCS projects in the Campos Basin, contributing to the overall understanding of CO_2 storage potential in this area.

The reservoir model has a pore volume of 150 billion m³. However, for the specific analysis in this work, a sector model from the offshore region with a smaller pore volume of approximately 160 million m³ is considered. The gridblock size is 100 m × 100 m horizontally and 5 m thick. The grid refinement technique based on the workflow proposed by Machado et al. [41] is used to refine the grid near the CO_2 injection well. The refinement is implemented to decrease the gridblock size from 100 m to 25 m near the injector. This adjustment aimed to improve the accuracy of representing the injection process and the trapping of CO_2, whether as an aqueous component or a residual phase in porous media, or as a free supercritical fluid.

The injection was evaluated for 20 years, from 2025 to 2045, with a constant injection rate of 1.0 million metric tonnes per year. A vertical injector was located in the center of the model in the bottom layers of the aquifer. It is important to note that in the selected area of the field, there is no evidence of an existing caprock (a layer of impermeable rock that can act as a barrier to prevent CO_2 leakage to out of the storage zone, such as a shallow freshwater aquifer). As a result, the main risk associated with this project is the buoyancy of CO_2 and the potential for leakage. Therefore, in this case, without the primary entrapment, it is crucial to address and quantify the uncertainty in the amount of CO_2 trapped by the secondary mechanisms (mainly, by solubility and hysteresis) in the aquifer to assess the feasibility and safety of the project.

Other properties of this actual reservoir model are summarized in Table 4.

Table 5 provides a summary of the uncertainty range considered for the trapping properties.
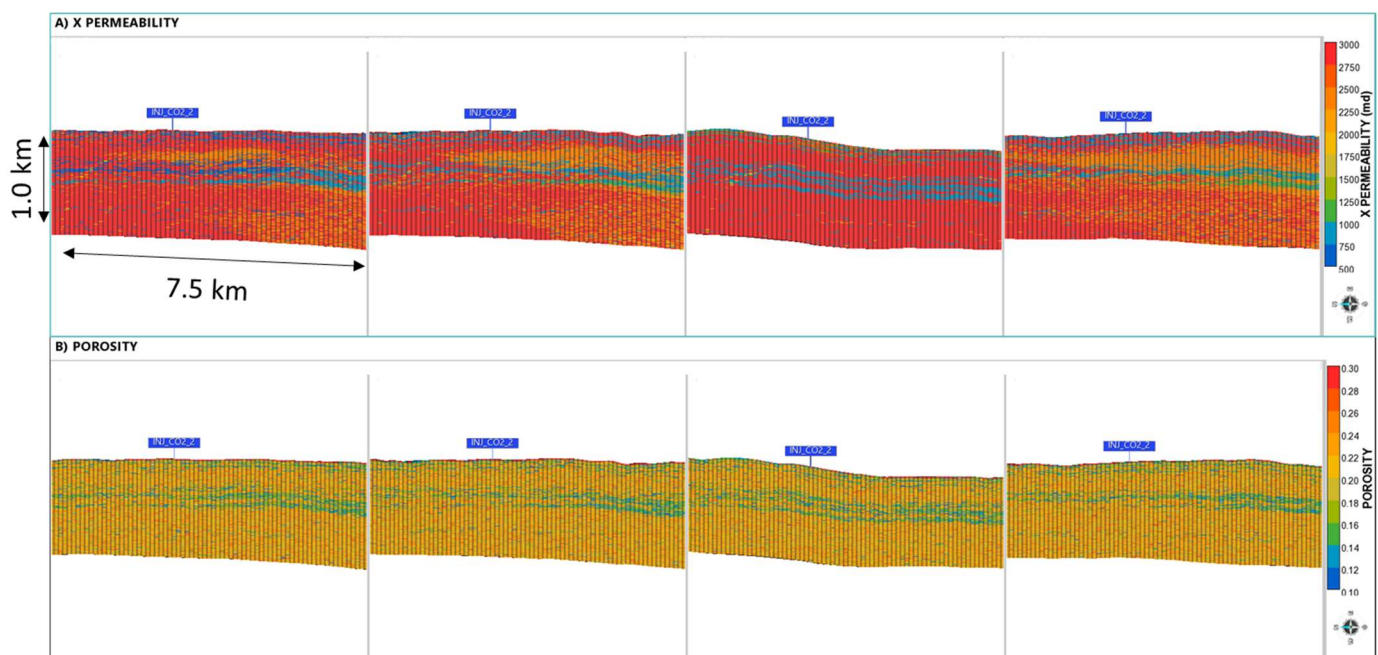
Table 4. Summary of reservoir properties.

Property	Value/Range
K_v/K_h ratio (continuous uniform distribution)	0.001 to 0.1
Initial pressure @ datum	7.159 MPa
Temperature	50 °C
Brine salinity	58,000 ppm
Initial pH	6.8
Brine composition	Table 2
Main minerals in the rock matrix (%vol)	Quartz (30%), K-feldspar (8%), Plagioclase (5%), and Calcite (1.1%)

A numerical experiment was conducted with 400 simulations using Latin Hypercube design [50]. These runs combined 75 heterogeneous realizations of permeability and porosity, the ratio of K_v/K_h distribution, and the trapping parameters listed in Table 5. The numerical experiment took approximately 1.5 days to complete the simulations, utilizing 20 parallel jobs on a computer cluster with 40 processors (Intel® Xeon® Gold 6230 CPU @ 2.10GHz, 104 GB RAM). Additionally, another set of 1000 runs was carried out to validate the response surface approach. These simulations required an additional 2 days to complete. The four objective functions (OF) that were evaluated are as follows:

- **II**: the CO_2 injectivity index after 20 years of injection;
- **Trapped_shutoff**: percentage of the total CO_2 injected that is trapped due to solubility, residual, and mineralization after the injection stops;
- **Trapped_30yr**: percentage of the total CO_2 injected that is trapped after 30 years of redistribution;
- **Trapped_100yr**: percentage of the total CO_2 injected that is trapped after 100 years of redistribution.

Table 5. Uncertainty range of the trapping properties.

Trapping Mechanism	Parameter	Range	Distribution	Source of the Lab Data that Supports the Distribution
Solubility/ Diffusion	H_i^*	2.91×10^5 to 3.69×10^5	Uniform	[23]
	Diffusion coefficient $CO_{2\ (aq)}$	3.5×10^{-5} to 4.0×10^{-5} cm²/s	Uniform	[25]
Residual Trapping	S_{gt}	Min = 0.1, Max = 0.52 and Most likely = 0.25	Triangular	[10]
	S_{wr}	0.15 to 0.5	Uniform	[10]
	Max CO_2 k_r	The logarithmic function of K		[10]
	k_r and P_c curves	Computed by correlation, with uniform distribution for: $S_{g\ crit}$: 0.02 to 0.1; n_g = 1 to 3; n_w = 1 to 3; *exp, d* and *exp, i*: 3 to 10.		[30,32–34]
	P_c values	Computed according to the gridblock permeability and porosity using J-function		[31]
Mineralization	Surface area: A	83.8–23,000 m²/m³	Uniform	[44]

Figure 7. Cross-sectional view with four examples of x-permeability (**A**) and porosity (**B**) scenarios. The injector's location is indicated by the blue box.

4. Discussion

Table 6 summarizes the simulation results (SR) and from 65,000 Monte Carlo simulations (MCS) using quadratic response surfaces [51] as proxy models to represent the SR for each objective function (OF). The last column in the table displays the respective R-squared (R^2) coefficient, which measures the reduction in the variability of the response achieved by using the regressor variables in the model.

It is worth noting that the maximum amount of CO_2 retention is reached after 30 years of redistribution. As a result, the uncertainty level calculated based on the ratio of P90 and P10 estimates, remains relatively constant at around 4 (in the 400-run case) and 3.5 (in the 1000-run case). In this context, the P90 represents the optimistic estimate for CO_2 storage, while the P10 represents the pessimistic estimate.

The errors between the SR and MCS results are found to be lower than 30%, with an R^2 higher than 80%, when considering 400 runs. These error levels are commonly observed in reservoir simulation applications, as mentioned in the study by Cremon et al. [52]. Therefore, they were considered sufficiently accurate for this study, considering the numerous variables involved.

Overall, the results obtained from the SR and MCS analyses, along with the R^2 coefficients, indicate that the proxy models built using quadratic response surfaces are reliable and provide satisfactory estimates for the objectives of this study.

Table 6. Stochastics estimates for the Objective Functions using SR and MCS, associated errors, P90/P10, and R^2.

Objective Function	Estimate	SR		MCS		Error SR and MCS (%)		P90/P10 (From MCS)		R^2 (%)	
		400 runs	1000 runs	400 runs	1000 runs	400 runs	1000 runs	400 runs	1000 runs	400 runs	1000 runs
"II" (kg/d-kPa)	P10	143	145	150	150	4.9	3.4				
	P50	185	185	184	184	0.5	0.5	1.33	1.33	80	80
	P90	200	200	200	200	0.0	0.0				
"Trapped_shutoff"	P10	13.3%	14.3%	14.6%	14.7%	10	2.8				
	P50	22.8%	23.1%	22.9%	23.0%	0.4	0.4	2.26	2.27	95	96
	P90	35.0%	34.3%	33.09%	33.3%	5.5	2.9				
"Trapped_30yr"	P10	16.5%	17.0%	13.23%	14.7%	19.7	13.5				
	P50	29.1%	28.9%	29.0%	28.8%	0.4	0.3	3.96	3.52	83	86
	P90	70.3%	55.7%	52.33%	51.7%	25.5	7.2				
"Trapped_100yr"	P10	16.1%	17.0%	13.23%	14.7%	17.9	13.5				
	P50	29.1%	28.9%	29.0%	28.8%	0.4	0.3	3.96	3.52	83	86
	P90	70.3%	56.0%	52.33%	51.7%	25.5	7.7				

The results indicate that the proxy models accurately predict the P50 estimate for the amount of CO_2 trapped and the injectivity index. However, there are significant discrepancies between the P10 and P90 estimates predicted by MCS and those obtained from the cumulative probability distribution derived from the SR in Figure 8. These differences are particularly notable after 30 and 100 years of CO_2 redistribution, with 400 simulation runs. This discrepancy leads to a reduction in the R^2 from 95% to 83% for proxy models. To address this issue and better represent cases with lower retention (close to the P10 estimate) and higher retention (close to the P90), additional simulation runs are performed. However, it requires a larger number of simulations in the order of one thousand to achieve satisfactory agreement with the results from other authors [52,53]. Nevertheless, it is worth noting that despite the need for a larger number of simulations, the P50 estimate is well predicted by the proxy model even with the limited number of 400 runs. The P50 estimate is typically considered for project evaluation and approval.
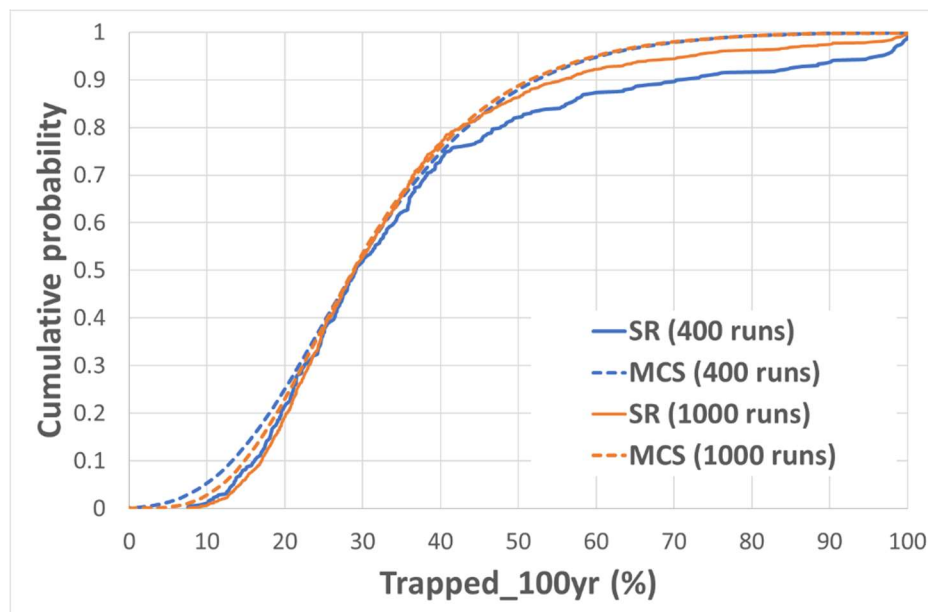

Figure 8. Cumulative probability functions from SR (solid lines) and MCS (dashed lines) for 400 (in blue) and 1000 runs (in orange).

Table 7 presents the distribution of CO_2 within the porous media for each uncertain scenario after 100 years. These distributions are calculated using MCS with a 1000-run case, and their respective R^2 values are also provided. The table reveals that in most scenarios, the majority of the CO_2 remains in a free state as a supercritical fluid. This finding highlights the potential risk of CO_2 leakage to the surface in CCS projects, particularly in geological scenarios where the caprock cannot effectively act as a barrier. In these scenarios, when there is a larger amount of free CO_2 present (P10), its plume has the potential to rise to shallower depths. This increases the risk associated with operations in areas that lack a caprock. Figure 9 illustrates the vertical distribution of CO_2 as a free phase in models that represent the three different estimates: P10 (minimum plume depth: 1569 m), P50 (2114 m), and P90 (2320 m). This information obtained from the uncertainty analysis is highly relevant as it highlights the potential risk of the CO_2 plume (under free CO_2 form) undesirably coming

into contact with shallow aquifers or even the sea floor (or surface in onshore targets). It underscores the importance of considering and managing these risks in CO_2 storage projects. The P90 case represents the lower-risk scenario, as more than 50% of the injected CO_2 is trapped, as shown in Table 7. Consequently, the free CO_2 plume remains at deeper depths (Figure 9). It is important to note that in the timeframe studied here, there is no significant CO_2 mineralized.
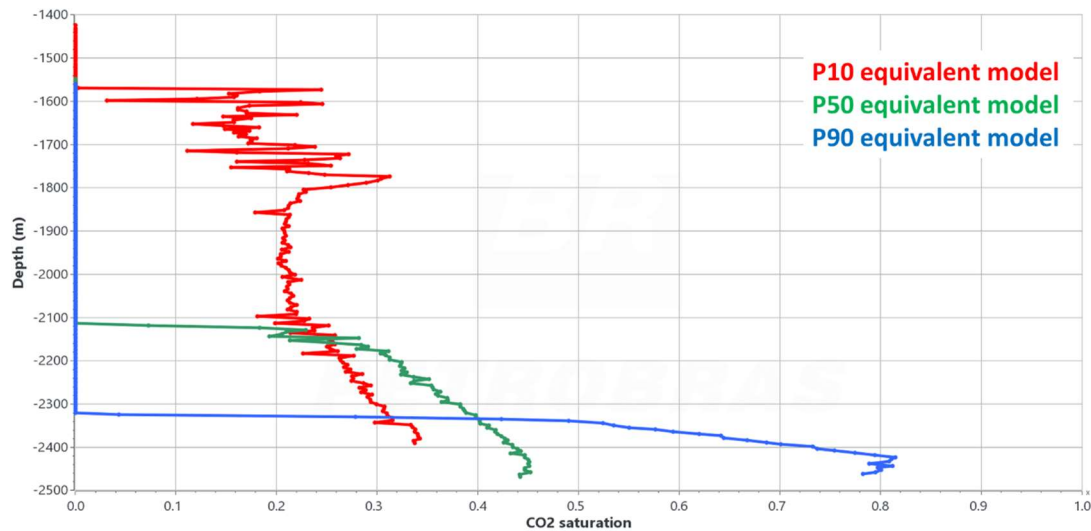

Figure 9. Depth of CO_2 plume rise from equivalent simulation models for P10 (in red), P50 (in green), and P90 (in blue) estimates.

Table 7. CO_2 inventory after 100 years of redistribution in porous media (OF: "Trapped_100yr").

After 100 Years of Redistribution	P10 (%)	P50 (%)	P90 (%)	R^2 (%)
Dissolved CO_2	8.5	18	39	80
Residual CO_2	8.5	11	17	84
Free CO_2	83	71	44	86

Figure 10 depicts the evolution of the percentage of CO_2 trapped over a span of 120 years. The green symbols in Figure 10 represent simulation results corresponding to the P50 estimate, while the vertical lines represent the range between the P10 and P90 equivalent models. These equivalent models are simulation models that yield results similar to those obtained using the proxy model estimation. The plot highlights that the uncertainty during the injection period is relatively small since the contributions from secondary trapping mechanisms of solubility, capillarity, and mineralization are insignificant. However, as the injection ceases, the importance of these mechanisms gradually increases as CO_2 redistributes within the porous media, which is consistent with Bachu [7]. This observation indicates that the uncertainty in CO_2 trapping becomes more pronounced and influential over time after the injection period concludes. In the P50 estimate, it is observed that a plateau is reached from year 50 onwards, indicating the maximum amount of CO_2 trapped through solubility and hysteresis. This suggests that 30 years of CO_2 redistribution was sufficient to achieve the maximum entrapment for the given system. However, it should be noted that this plateau may vary if more optimistic (P90) or pessimistic (P10) trapping properties are assumed.

MCS can also be employed to investigate the most influential parameters for CO_2 retention. The effect estimated in a Tornado plot quantifies how a parameter (and some modification in its value) can impact the objective function (OF). By definition, the effect of an individual parameter on the OF is referred to as a main (or first-order) effect. However, interaction effects consider the combinations of model parameters that cannot be described by the first-order effects only [54]. In this particular problem, interactions are important and integral aspects of the models, such as those between relative permeability (k_r) and capillary pressure (P_c) parameters such as residual saturations and relative permeability endpoint and exponents (S_{gt}, S_{wr}, $S_{g\ crit}$, n_g, and Max $CO_2\ k_r$, as well as the petrophysical properties (K, ϕ, and K_v/K_h) derived from the geological models.

Figure 11 presents the Top-7 most significant parameters and their associated interactions (represented by orange bars), which add up to 100% for the "Trapped_100yr" OF. If a linear response surface is employed as a proxy model, the R^2 value reduces from 86% to 66% (in the case of 1000 runs), indicating the importance of capturing the interaction effects represented by the quadratic surface. This finding aligns with the conclusions of Khanal and Shahriar [16], who employed advanced machine-learning techniques to construct proxy models. Although their models had higher R^2 values than the results of this work, they considered only seven input parameters and made simplified assumptions, i.e., no uncertainty in solubility, no capillarity effects, and the use of a single set of relative permeability curves.
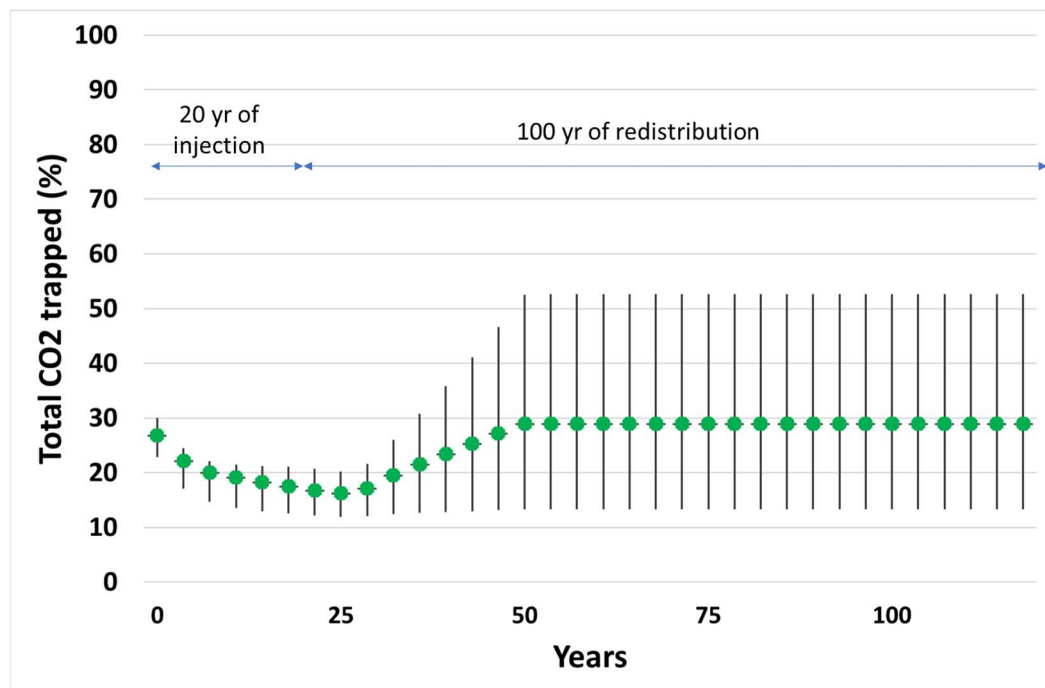
Figure 10. Evolution of the % CO_2 trapped over 20 years of injection and 100 years of redistribution. Green dots are the P50 estimate, the vertical black lines represent the variation between P10 and P90.
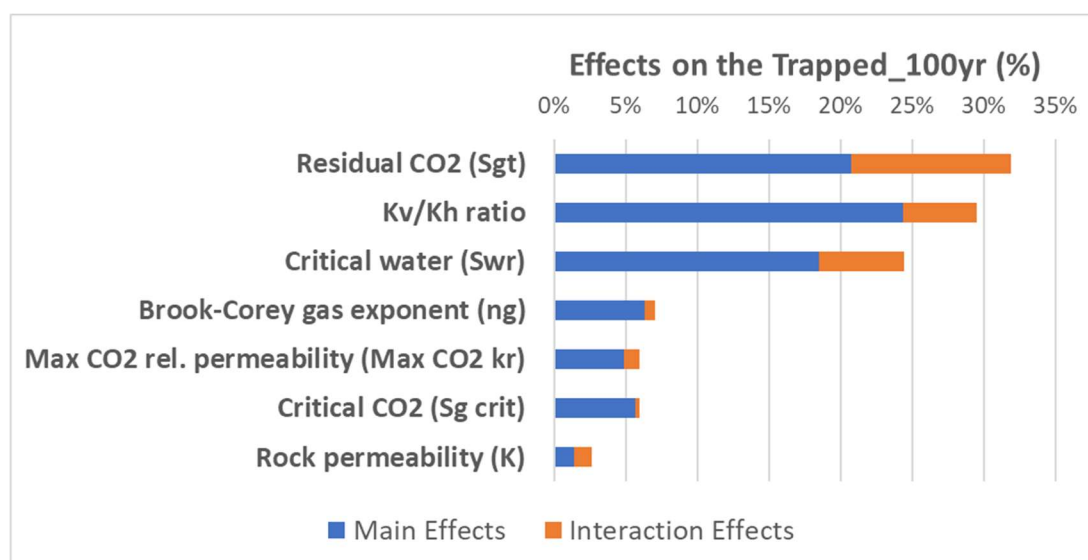

Figure 11. Tornado plot for the Objective Function "Trapped_100 yr" generated with MCS calibrated with 1000 runs.

In Figure 11, the solubility parameter H_i^* did not appear as a significant property for the objective function "Trapped_100yr". This can be attributed to the narrow range (lower uncertainty) of the solubility parameter in the 58,000 ppm case, where the model prediction aligns well with the laboratory data, as shown in Figure 1. However, if a higher salinity case (230,000 ppm) is used, where the difference between the initial prediction and the data is more significant (as depicted in Figure 2), H_i^* will have a main effect of 3.7% on the "Trapped_100yr" objective function, indicating a significant uncertainty in solubility. These observations emphasize the importance of evaluating the uncertainty in the solubility model calculations.

Figure 12 displays the Tornado Plot for "II" at the time of injection shutoff, specifically regarding CO_2 injectivity. These results support the findings of Machado et al. [35], which concluded that residual CO_2 saturation does not significantly impact injectivity. Essentially, the injectivity of CO_2 is influenced by its effective permeability, which is determined by the product of the maximum CO_2 relative permeability (*Max CO_2 k_r*) and the absolute permeability in both the horizontal (*K*) and vertical directions. The vertical permeability plays a critical role in enhancing CO_2 buoyancy, which in turn facilitates its redistribution within porous media and increases its saturation. This amplification of CO_2 saturation ultimately leads to an enhanced mobility of CO_2 within the porous media, positively impacting its injectivity. The

significant influence of geological properties on injectivity emphasizes the importance of the proposed methodology, which integrates different geological scenarios. Furthermore, Figure 12 indicates that the reactive calcite area, denoted as *A*, does not have a substantial effect because of small percentage of calcite of 1.1% present in the reservoir rock.

The steps followed in the proposed workflow can be summarized by referring to the flowchart presented in Figure 13. The flowchart illustrates the integration of geological scenarios and trapping mechanisms, supported by experimental measurements, to map the fate of CO_2 in porous media. This comprehensive approach enables a more precise assessment of the potential impacts of geological and trapping properties on CO_2 injectivity and entrapment. Ultimately, it facilitates informed decision-making in CCS projects.
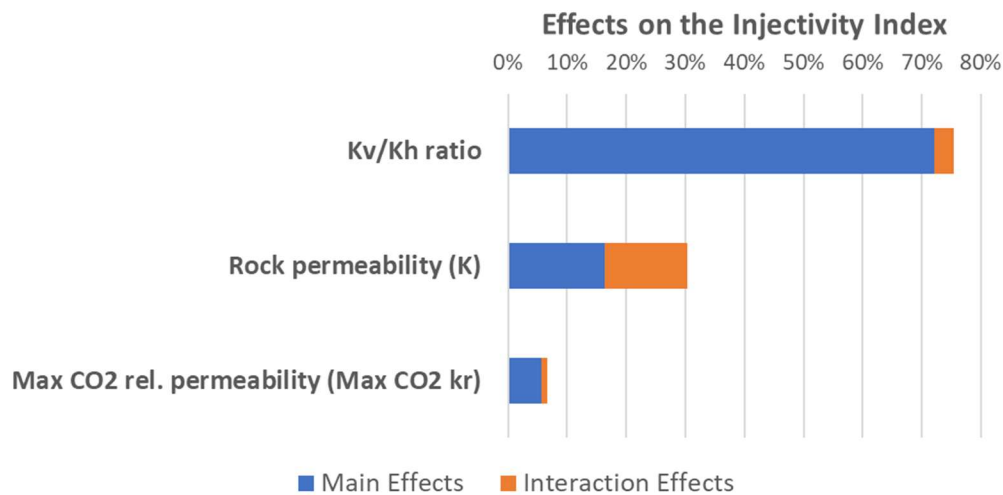

Figure 12. Tornado plot for the OF "II" generated with MCS calibrated with 1000 runs.
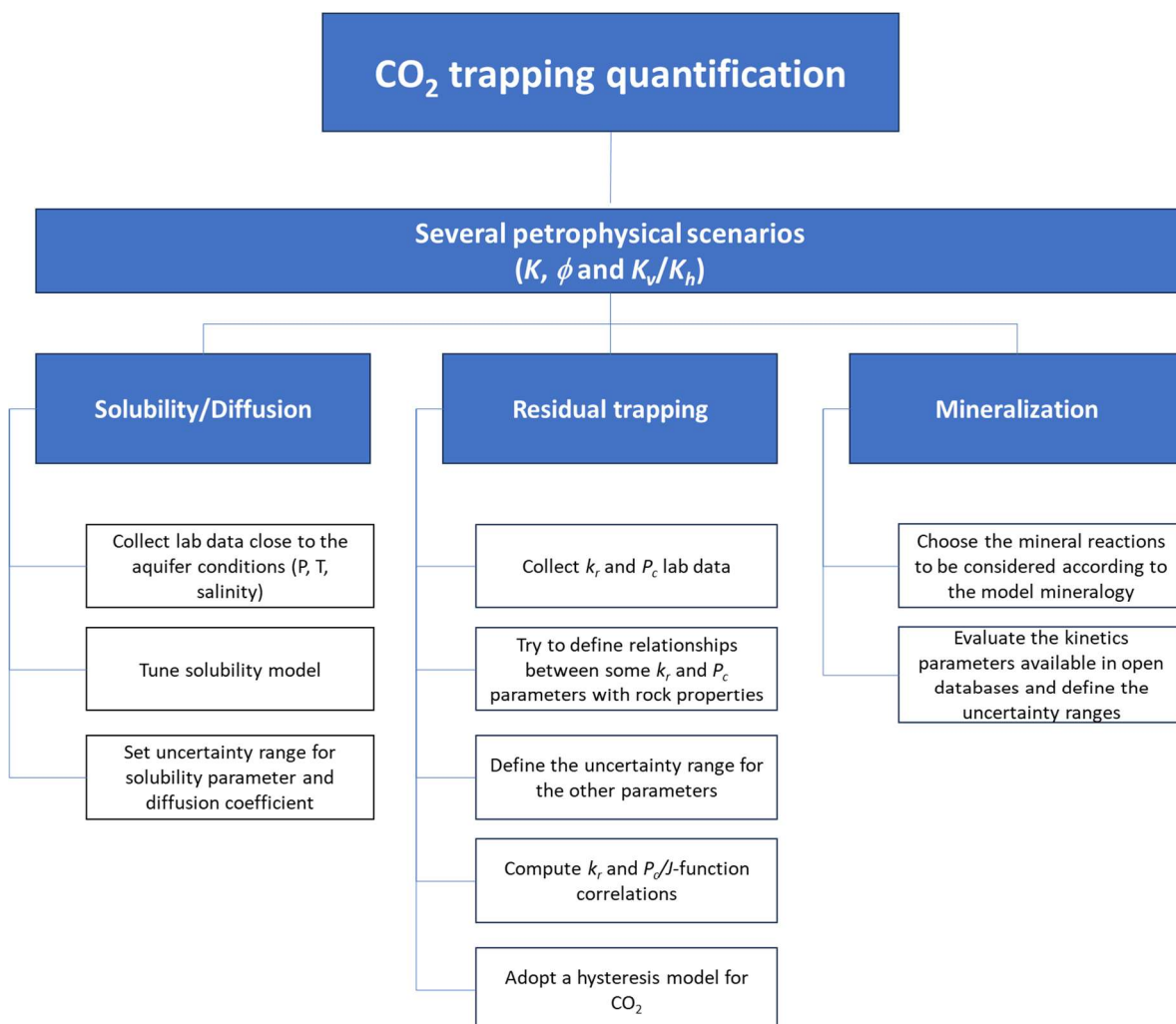

Figure 13. Flowchart with main steps for uncertainty analysis in CCS projects.

5. Conclusions

In conclusion, the uncertainty analysis conducted in this study, despite being based on a specific target with a geological model under different scenarios, allows for the expansion and generalization of the proposed workflow. This analysis provides valuable insights for project evaluation, particularly regarding the main subsurface risks associated with CCS operations. The main conclusions of this study can be summarized as follows:

Regarding the experimental data:

- Laboratory-measured data for parameters that control CO_2 retention in porous media should be used in order to guide the input distribution for uncertainty assessment. This helps to more accurately map their impacts on the resulting trapped CO_2 over time.

Regarding the uncertainty assessment on the CO_2 trapping:

- The workflow employed in this study successfully mapped the uncertainty associated with the amount of CO_2 trapped. This mapping is crucial for determining appropriate mitigation measures to address the risk of leakage in storage targets where the caprock may not serve as an effective barrier. It enables the evaluation of the feasibility of CCS operations in such targets and aids in making informed decisions.
- The results obtained from a geological model of an actual saline sandstone aquifer demonstrated significant variations in CO_2 trapping, ranging from 17% for the P10 estimate to 56% for the P90 estimate. In the P50 estimate, the CO_2 entrapment reached a plateau of approximately 29% after 30 years following the cessation of injection. This highlights the importance of considering uncertainty during the risk assessment and approval phases of CO_2 storage projects.
- Proxy models constructed using quadratic response surfaces were able to accurately represent the objective functions used to evaluate CO_2 injectivity and retention over different time periods in the P50 estimate. These models performed well even with a relatively small number of runs (400), making them valuable tools for decision-making.
- Although the proxy models for the P10 and P90 estimates can benefit from further improvements, obtaining a larger number of additional simulations (more than 600 cases) can be challenging, especially for larger models.
- Tornado plots revealed a strong interplay between reservoir properties (such as permeability - K -, and the ratio of vertical to horizontal permeability - K_v/K_h) and dynamic petrophysical parameters (such as S_{gt}, S_{wr}, $S_{g\ crit}$, n_g, and Max CO_2 k_r) in determining the amount of CO_2 trapped as an objective function. This underscores the importance of an integrated workflow for uncertainty and risk evaluation.

Regarding the uncertainty assessment on the CO_2 injectivity:

- The low reactivity of minerals in the rock matrix led to a negligible impact of mineral trapping, primarily attributed to calcite dissolution. However, this influence was not significant enough to affect CO_2 injectivity;
- By coupling the methodology with geological considerations, a more comprehensive understanding of the injectivity process can be achieved. The results highlight the greater influence of geological properties, such as the K_v/K_h ratio and absolute permeability, compared to trapping parameters.

For future research, the authors recommend and intend to expand the geochemical modeling in the uncertainty evaluation to apply to targets where the matrix contains more reactive minerals. In this regard, the modeling of water vaporization and halite scale should be considered for a more representative and comprehensive study.

Nomenclature

A: reactive surface area, m^2/m^3;
exp: exponent for the capillary pressure correlation, dimensionless;
E_a: activation energy, J/mol;
H_i: Henry's constant at current pressure (p) and temperature (T), dimensionless;
H_i^*: Henry's constant at reference pressure (p^*) and temperature (T), dimensionless;
J: Leverett J-function, dimensionless;
K: rock permeability, mD;
K_{eq}: chemical equilibrium constant, dimensionless;
k_{25}: rate constant at 25°C, mol/m^2s;
k_{rl}: relative permeability for phase l, dimensionless;
n_g: CO_2 k_r curve exponent in Brooks-Corey model, dimensionless;
n_w: water k_r curve exponent in Brooks-Corey model, dimensionless;
P_c: CO_2-brine capillary pressure, kPa;
R: universal gas constant, 8.314 kPa·L/mol·K;

S_{gt}: residual gas saturation due to hysteresis, dimensionless (vol/vol);
$S_{g\,crit}$: critical gas saturation, dimensionless (vol/vol);
S_l: current fluid saturation, dimensionless (vol/vol);
S_{wr}: residual water saturation, dimensionless (vol/vol);
$\bar{v}_l$: partial molar volume at infinite dilution, L/mol;

Greek symbols

ϕ: rock porosity;

Subscripts

d: drainage;
i: imbibition;
l: fluid (w – water or CO_2);
h: horizontal;
v: vertical.

Acronyms

EoS: equation-of-state;
CCS: carbon capture and storage;
II: injectivity index;
MCS: Monte Carlo simulation;
OF: objective function;
SR: simulation results.

Acknowledgments

Author Contributions

Conceptualization, M.V.B.M., M.D. and K.S.; methodology, M.V.B.M.; software, M.V.B.M.; validation, M.V.B.M., M.D. and K.S.; formal analysis, M.V.B.M., M.D. and K.S.; investigation, M.V.B.M.; resources, M.V.B.M. and M.D.; data curation, M.V.B.M. and M.D.; writing—original draft preparation, M.V.B.M.; writing—review and editing, M.D. and K.S.; visualization, M.V.B.M.; supervision, M.D. and K.S.; project administration, M.D. and K.S. All authors have read and agreed to the published version of the manuscript.

Ethics Statement

Not applicable.

Informed Consent Statement

Not applicable.

Funding

Declaration of Competing Interest

The authors declare that they have no known competing financial interests or personal relationships that could have appeared to influence the work reported in this paper.

References

1. Birol DF. *World Energy Outlook 2022*; IEA: Paris, France 2022.
2. Nghiem L, Shrivastava V, Kohse B, Hassam M, Yang C. Simulation of Trapping Processes for CO_2 Storage in Saline Aquifers. In Proceedings of the Canadian International Petroleum Conference, Calgary, Alberta, June 2009.
3. Han WS, McPherson BJ, Lichtner PC, Wang FP. Evaluation of Trapping Mechanisms in Geologic CO_2 Sequestration: Case Study of SACROC Northern Platform, a 35-Year CO_2 Injection Site. *Am. J. Sci.* **2010**, *310*, 282–324.
4. Delshad M, Kong X, Tavakoli R, Hosseini SA, Wheeler MF. Modeling and Simulation of Carbon Sequestration at Cranfield Incorporating New Physical Models. *Int. J. Greenh. Gas Control* **2013**, *18*, 463–473.
5. Rackley SA. *Carbon Capture and Storage*, 2nd ed.; Butterworth-Heinemann: Cambridge, MA, USA, 2017.

6. Machado MVB, Delshad M, Sepehrnoori K. Potential Benefits of Horizontal Wells for CO_2 Injection to Enhance Storage Security and Reduce Leakage Risks. *Appl. Sci.* **2023**, *13*, 12830.

7. Bachu S. CO_2 Storage in Geological Media: Role, Means, Status and Barriers to Deployment. *Progress Energy Combust. Sci.* **2008**, *34*, 254–273.

8. Dodds WS, Stutzman LF, Sollami BJ. Carbon Dioxide Solubility in Water. *Ind. Eng. Chem. Chem. Eng. Data Series* **1956**, *1*, 92–95.

9. Duan Z, Sun R. An Improved Model Calculating CO_2 Solubility in Pure Water and Aqueous NaCl Solutions from 273 to 533 K and from 0 to 2000 Bar. *Chem. Geol.* **2003**, *193*, 257–271.

10. Burnside NM, Naylor M. Review and Implications of Relative Permeability of CO_2/Brine Systems and Residual Trapping of CO_2. *Int. J. Greenh. Gas Control* **2014**, *23*, 1–11.

11. Xu T, Yue G, Wang F, Liu N. Using Natural CO_2 Reservoir to Constrain Geochemical Models for CO_2 Geological Sequestration. *Appl. Geochem.* **2014**, *43*, 22–34.

12. Machado MVB. *Modelagem Numérica de Reservatórios de Petróleo: Prática Integrada de Simulação*; Petrobras: Rio de Janeiro, Brazil, 2023.

13. Tadjer A, Bratvold RB. Managing Uncertainty in Geological CO_2 Storage Using Bayesian Evidential Learning. *Energies* **2021**, *14*, 1557.

14. Mahjour SK, Faroughi SA. Selecting Representative Geological Realizations to Model Subsurface CO_2 Storage under Uncertainty. *Int. J. Greenh. Gas Control* **2023**, *127*, 103920.

15. Raza Y. Uncertainty Analysis of Capacity Estimates and Leakage Potential for Geologic Storage of Carbon Dioxide in Saline Aquifers. Master's Thesis, Massachusetts Institute of Technology: Cambridge, MA, USA, 2006.

16. Khanal A, Shahriar MF. Physics-Based Proxy Modeling of CO_2 Sequestration in Deep Saline Aquifers. *Energies* **2022**, *15*, 4350.

17. Jammoul M, Delshad M, Wheeler MF. Numerical Modeling of CO_2 Storage: Applications to the FluidFlower Experimental Setup. *Transp. Porous. Med.* **2023**. doi:10.1007/s11242-023-01996-4.

18. Likanapaisal P, Lun L, Krishnamurthy P, Kohli K. Understanding Subsurface Uncertainty for Carbon Storage in Saline Aquifers: PVT, SCAL, and Grid-Size Sensitivity. In Proceedings of the SPE Annual Technical Conference and Exhibition, San Antonio, Texas, USA, October 2023.

19. Li Y-K, Nghiem LX. Phase Equilibria of Oil, Gas and Water/Brine Mixtures from a Cubic Equation of State and Henry's Law. *Can. J. Chem. Eng.* **1986**, *64*, 486–496.

20. Harvey AH, Prausnitz JM. Thermodynamics of High-Pressure Aqueous Systems Containing Gases and Salts. *AIChE J.* **1989**, *35*, 635–644.

21. CMG. *GEM Compositional & Unconventional Simulator* (version 2022.10); Windows; CMG: Calgary, AB, Canada, 2022.

22. Bakker RJ. Package FLUIDS 1. Computer Programs for Analysis of Fluid Inclusion Data and for Modelling Bulk Fluid Properties. *Chem. Geol.* **2003**, *194*, 3–23.

23. Yan W, Huang S, Stenby EH. Measurement and Modeling of CO_2 Solubility in NaCl Brine and CO_2–Saturated NaCl Brine Density. *Int. J. Greenh. Gas Control* **2011**, *5*, 1460–1477.

24. Rezk MG, Foroozesh J, Abdulrahman A, Gholinezhad J. CO_2 Diffusion and Dispersion in Porous Media: Review of Advances in Experimental Measurements and Mathematical Models. *Energy Fuels* **2022**, *36*, 133–155.

25. Ahmadi H, Erfani H, Jamialahmadi M, Soulgani BS, Dinarvand N, Sharafi MS. Corrigendum to "Experimental Study and Modelling on Diffusion Coefficient of CO_2 in Water" Fluid Phase Equilibria 523 (2020) 112,584. *Fluid Phase Equilibria* **2021**, *529*, 112869.

26. Perera PN, Deng H, Schuck PJ, Gilbert B. Diffusivity of Carbon Dioxide in Aqueous Solutions under Geologic Carbon Sequestration Conditions. *J. Phys. Chem. B* **2018**, *122*, 4566–4572.

27. Carlson FM. Simulation of Relative Permeability Hysteresis to the Nonwetting Phase. In Proceedings of the SPE Annual Technical Conference and Exhibition, San Antonio, TX, USA, 4 October 1981.

28. Land CS. Calculation of Imbibition Relative Permeability for Two- and Three-Phase Flow from Rock Properties. *Soc. Petrol. Eng. J.* **1968**, *8*, 149–156.

29. Jarrell PM. *Practical Aspects of CO_2 Flooding*; Society of Petroleum Engineers: Richardson, TX, USA, 2002.

30. Brooks RH, Corey AT. Properties of Porous Media Affecting Fluid Flow. *J. Irrig. and Drain. Div.* **1966**, *92*, 61–88.

31. Leverett MC. Capillary Behavior in Porous Solids. *Trans. AIME* **1941**, *142*, 152–169.

32. Bennion DB, Bachu S. Drainage and Imbibition Relative Permeability Relationships for Supercritical CO_2/Brine and H_2S/Brine Systems in Intergranular Sandstone, Carbonate, Shale, and Anhydrite Rocks. *SPE Reserv. Eval. Eng.* **2008**, *11*, 487–496.

33. Krevor SCM, Pini R, Zuo L, Benson SM. Relative Permeability and Trapping of CO_2 and Water in Sandstone Rocks at Reservoir Conditions. *Water Resour. Res.* **2012**, *48*, 2011WR010859.

34. Jung J, Hu JW. Impact of Pressure and Brine Salinity on Capillary Pressure-Water Saturation Relations in Geological CO_2 Sequestration. *Adv. Condens. Matter Phys.* **2016**, *2016*, 1–11.

35. Machado MVB, Delshad M, Sepehrnoori K. Injectivity Assessment for CCS Field-Scale Projects with Considerations of Salt Deposition, Mineral Dissolution, Fines Migration, Hydrate Formation, and Non-Darcy Flow. *Fuel* **2023**, *353*, 129148.

36. Melrose JC. Valid Capillary Pressure Data at Low Wetting-Phase Saturations. *SPE Reserv. Eng.* **1990**, *5*, 95–99.

37. Xiao Y, Xu T, Pruess K. The Effects of Gas-Fluid-Rock Interactions on CO_2 Injection and Storage: Insights from Reactive Transport Modeling. *Energy Procedia* **2009**, *1*, 1783–1790.

38. Parkhurst DL, Thorstenson DC, Plummer LN. *PHREEQE: A Computer Program for Geochemical Calculations*; U.S. Geological Survey: Denver, CO, USA, 1980.

39. Parkhurst DL, Appelo CAJ. *Description of Input and Examples for PHREEQC Version 3: A Computer Program for Speciation, Batch-Reaction, One-Dimensional Transport, and Inverse Geochemical Calculations.*; U.S. Geological Survey Techniques and Methods, Book 6; U.S. Geological Survey: Denver, CO, USA, 2013; p. 497.

40. Lasaga AC. Chemical Kinetics of Water-Rock Interactions. *J. Geophys. Res.* **1984**, *89*, 4009–4025.

41. Machado MVB, Delshad M, Sepehrnoori K. A Practical and Innovative Workflow to Support the Numerical Simulation of CO_2 Storage in Large Field-Scale Models. *SPE Reserv. Eval. Eng.* **2023**, *26*, 1541–1552.

42. Allison JD, Brown DS, Novo-Gradac KJ. *MINTEQA2/PRODEFA2: A Geochemical Assessment Model for Environmental Systems: Version 3.0 User's Manual*; EPA: Washington, DC, USA, 1991.

43. Wolery TJ. *EQ3/6, a Software Package for Geochemical Modeling of Aqueous Systems: Package Overview and Installation Guide (Version 7.0)*; USDOE: Washington, DC, USA, 1992.

44. Luo S, Xu R, Jiang P. Effect of Reactive Surface Area of Minerals on Mineralization Trapping of CO_2 in Saline Aquifers. *Pet. Sci.* **2012**, *9*, 400–407.

45. Bolourinejad P, Shoeibi Omrani P, Herber R. Effect of Reactive Surface Area of Minerals on Mineralization and Carbon Dioxide Trapping in a Depleted Gas Reservoir. *Int. J. Greenh. Gas Control* **2014**, *21*, 11–22.

46. Chen H, Wang C, Ye M. An Uncertainty Analysis of Subsidy for Carbon Capture and Storage (CCS) Retrofitting Investment in China's Coal Power Plants Using a Real-Options Approach. *J. Clean. Prod.* **2016**, *137*, 200–212.

47. Koelbl BS, Van Den Broek MA, Faaij APC, Van Vuuren DP. Uncertainty in Carbon Capture and Storage (CCS) Deployment Projections: A Cross-Model Comparison Exercise. *Clim. Change* **2014**, *123*, 461–476.

48. Van Der Spek M, Fout T, Garcia M, Kuncheekanna VN, Matuszewski M, McCoy S, et al. Uncertainty Analysis in the Techno-Economic Assessment of CO_2 Capture and Storage Technologies. Critical Review and Guidelines for Use. *Int. J. Greenh. Gas Control* **2020**, *100*, 103113.

49. Oda J, Akimoto K. An Analysis of CCS Investment under Uncertainty. *Energy Procedia* **2011**, *4*, 1997–2004.

50. Mckay MD, Beckman RJ, Conover WJ. A Comparison of Three Methods for Selecting Values of Input Variables in the Analysis of Output from a Computer Code. *Technometrics* **2000**, *42*, 55–61.

51. Ma YZ. *Quantitative Geosciences: Data Analytics, Geostatistics, Reservoir Characterization and Modeling*; Springer International Publishing: Cham, Switzerland, 2019.

52. Cremon MA, Christie MA, Gerritsen MG. Monte Carlo Simulation for Uncertainty Quantification in Reservoir Simulation: A Convergence Study. *J. Petrol. Sci. Eng.* **2020**, *190*, 107094.

53. Ballio F, Guadagnini A. Convergence Assessment of Numerical Monte Carlo Simulations in Groundwater Hydrology: TECHNICAL NOTE. *Water Resour. Res.* **2004**, *40*, W04603.

54. Saltelli A, Ratto M, Andres T, Campolongo F, Cariboni J, Gatelli D, et al. *Global Sensitivity Analysis. The Primer*, 1st ed.; Wiley: Wiley: Hoboken, NJ, USA, 2007.